SPM Response of a Distributed Coupling Coefficient DFB-SOA All-Optical Flip-Flop

M. Jabbari[1], M.K. MoravvejFarshi[2], R. Ghayour[3], A. Zarifkar[4]
1- Department of Electrical Engineering, Islamic Azad University, Marvdasht Branch, Marvdasht, Iran,
Email: jabbari@miau.ac.ir
2- Department of Electrical Engineering, Tarbiat Modares University, Tehran, Iran,
Email: farshi_k@modares.ac.ir
3- Department of Electrical Engineering, Shiraz University, Shiraz, Iran,
Email: rghayour@shirazu.ac.ir
4- Iran Telecomm Research Center, Tehran, Iran,
Email: azarifkar@itrc.ac.ir

Received: August 2009 Revised: October 2009 Accepted: December 2009

ABSTRACT:
Deriving a dynamic model based on the coupled-mode and carrier rate equations, the effects of coupling coefficient and corrugation position on all-optical flip-flops (AOFF) we have analyzed in this paper. Also the self phase modulation (SPM) in the distributed coupling coefficient distributed feedback semiconductor optical amplifier (DCC-DFB-SOA) has been implemented. Then the effects of SPM on the rise and fall times of the flip-flop DFB-SOA are investigated. It has been shown that the application of the optimized coupling coefficient and corrugation position improves the speed limitation in AOFF significantly. The transfer matrix method (TMM) time domain is utilized for the numerical simulations.

KEYWORDS: All-Optical Flip-Flops (AOFF), Distributed Coupling Coefficient (DCC), Distributed Feedback (DFB), Semiconductor Optical Amplifier (SOA), Self Phase Modulation (SPM).

1. INTRODUCTION

Optical packet switching has been intensely investigated to meet the future's great demand for data traffic due to its high bandwidths, efficiency and throughput. In an all-optical packet switch, after taking the optical label from the injected optical packet, the optical label is converted to a parallel signal and applied to the optical flip-flop. The optical outputs from the flip-flop enter the all-optical switches [1]. Thus, in such systems, optical packets are switched in a fully optical domain without any optoelectronic conversion. Ultra fast switching can be achieved by this configuration due to its high speed operation of both the optical flip-flop and full-optical switches [1]. In addition, the latching capability of a full optical flip–flop will allow the output to be maintained for processing at a later time. This capability can be used in sequential process such as bit-length conversion, data-format change, de-multiplexing and re-timing schemes [2]. Recently, different all-optical flip-flops (AOFFs) have been proposed where their well known mechanisms are: the distributed feedback semiconductor optical amplifier (DFB-SOA) [2], the semiconductor optical amplifier (SOA) mutually connected with a DFB-laser diode [3-5], and the optical bistability in an integrated SOA and DFB-SOA [6].

A DFB semiconductor laser diode, when biased below its lasing threshold, acts as a distributed coupling coefficient DFB-SOA (DCC-DFB-SOA) and shows dispersive optical bistability behavior [7]. This device suffers from low speed due to its high carrier life time. Although this intrinsic carrier life time is in the order of few hundred picoseconds, the effective carrier lifetime can be decreased by stimulated emission significantly [8]. Reducing the effective carrier life time can be achieved by increasing the photon number in the DCC-DFB-SOA.

In this paper, for the first time, we have presented a numerical investigation of the dynamic response of a flip-flop DCC-DFB-SOA (FF-DCC-DFB-SOA) based on self phase modulation (SPM).

2. DCC-DFB-SOA STRUCTURE

In order to study the fundamental characteristics of all-optical flip-flops (AOFF) a DCC-DFB-SOA operating at 1550nm is considered. The active region

consists of a stripe 2μm wide and 150nm thick. Its length is considered to be a design parameter. It (What is this "it"?) is assumed to support a single transverse mode. Figure 1 illustrates the schematic diagram of a DCC-DFB-SOA. The height of the corrugations in the middle of the cavity is considered to be different from those of the left and right sections. Hence, the coupling coefficient in the middle section of the SOA cavity, κ2, differs from that representing both the left and right sections, κ1. In this analysis, throughout the cavity length a constant period of Λ has been assumed for the corrugations and hence a fixed Bragg wavelength λB [9].

3. THEORETICAL BACKGROUND

The time-domain traveling wave model based on the coupled wave equations is well established for the simulation of DFB structures. In the spatial domain, such devices exhibit non-uniform carrier and photon distributions along the propagating direction. Therefore, the governing equations have to be discretized along the active layer in a DCC-DFB-SOA to treat these variations. Obviously, these equations and the discretization scheme can also be adopted to describe the processes in SOA [10]. The DFB structures are normally designed for single-mode operation. Therefore, it is sufficient to solve the governing equations only in a narrow spectral range near the lasing wavelength where the phase information is preserved. The electric field in this type of waveguide is expressed as:

$$E(x,y,z;t) = \varphi(x,y)[F(z,t)e^{-j\beta_0 z} + R(z,t)e^{j\beta_0 z}]\times e^{j\omega t} \quad (1)$$

Where $\beta 0=\pi/\Lambda$ is the propagation constant at the Bragg wavelength, Λ is the grating period, ω is the reference frequency, and $\varphi(x,y)$ is the transverse field profile. $F(z, t)$ and $R(z, t)$ represent complex electric field envelopes of forward and backward travelling waves, respectively. Substituting (1) into Maxwell's equations yields the following time-dependent coupled wave equations governing the lasing mode field which propagates in the active layer of the DFB-SOA,

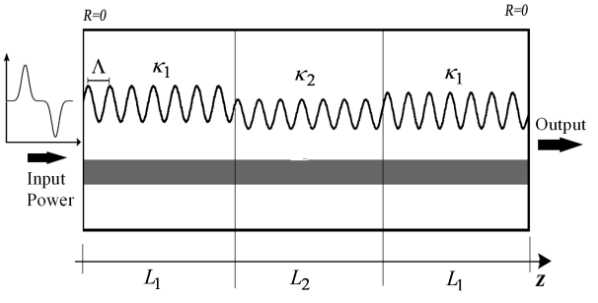

Fig. 1. Schematic diagram of DCC-DFB-SOA

$$\frac{1}{v_g}\frac{\partial F(z,t)}{\partial t}+\frac{\partial F(z,t)}{\partial z} = \left\{-j\delta+\frac{1}{2}\left(\Gamma g(z,t)-\alpha_s\right)\right\}F(z,t)+j\kappa(z)R(z,t) \quad (2a)$$

$$\frac{1}{v_g}\frac{\partial R(z,t)}{\partial t}-\frac{\partial R(z,t)}{\partial z} = \left\{-j\delta+\frac{1}{2}\left(\Gamma g(z,t)-\alpha_s\right)\right\}R(z,t)+j\kappa(z)F(z,t) \quad (2b)$$

Where v_g is the group velocity, α_s accounts for the internal loss which is assumed to be negligible, and $\kappa(z)$ denotes the coupling coefficient of the grating. We have ignored the impact of amplified spontaneous emission (ASE), which is justified for larger input power. In order to facilitate the comparison of the results obtained by the present approach with other approaches a parameter known as the averaged coupling coefficient, κ_{av}, has been introduced for this DCC-DFB-SOA structure such that:

$$\kappa_{av} = \kappa_1 \cdot r_L + \kappa_2 (1 - r_L) \quad (3)$$

Where $r_L = 2L_1 / L$. For given values of κ_{av}, the coupling ratio $r_\kappa = \kappa_1 / \kappa_2$, (3) reduces to,

$$\kappa_1 = \frac{r_\kappa \cdot \kappa_{avg}}{1+(r_\kappa - 1)r_L} \quad (4)$$

Where κ_1 can be determined. The phase detuning factor from the Bragg wavelength is given as [10]:

$$\delta = \beta(\lambda_s) + \frac{1}{2}\alpha_m g(z,t) - \beta_0 \quad (5)$$

Where $\beta(\lambda_s)=2\pi n_{eff}/\lambda_s$ is the signal propagation constant and λ_s is the signal wavelength, αm denotes the line-width enhancement factor, and $g(z,t)$ is the material gain which depends on the carrier density, $N(z,t)$, given by [11]:

$$g(z,t) = a[N(z,t) - N_0] \quad (6)$$

Where $a=dg/dN$ is the differential gain, and N_0 is the transparency carrier concentration. Here, it has been assumed that the gain peak wavelength is consistent with the input wavelength, and its shift with carrier

density has also been ignored [8]. For an active layer which thickness *(d)* and width *(W)* are both larger than the carrier diffusion length, the carrier density rate equation becomes:

$$\frac{\partial N(z,t)}{\partial t} = \frac{J}{qd} - \frac{N(z,t)}{\tau_{eff}(z,t)} - g(z,t)\Gamma\frac{\sigma}{\hbar\omega Wd}\left[|F(z,t)|^2 + |R(z,t)|^2\right] \quad (7)$$

Where L is the cavity length, q is the electronic charge, $J=I/WL$ is the current density, σ is the mode cross section, Γ is the confinement factor, $\hbar$ is the reduced Planck constant, ω is the light radian frequency, and τ_{eff} is the effective carrier lifetime given by

$$\tau_{eff}(z,t) = \frac{\tau_c}{1+\frac{\Gamma a\tau(z,t-1)\sigma}{\hbar Wd}\left[\frac{(|F(z,t)|^2+|R(z,t)|^2}{\omega}\right]} \quad (8)$$

In which τ_c is the carrier lifetime,

$$\tau_c = \left\{A_{nard} + B_{rad}N(z,t) + C_{Aug}N^2(z,t)\right\}^{-1} \quad (9)$$

Where A_{nrad} is the non-radiative recombination rated due to Shockley-Read-Hall (SRH) process, B_{rad} is the total radiative recombination rate, and C_{Aug} is the total Auger recombination rate. To achieve transparency condition, the rate equation is solved in steady state condition with Newton–Raphson technique, in which N_0 is a given value.

4. SIMULATION RESULTS

In our simulation, we assumed that the duration of the input pulse is much longer than the round-trip time in cavity. Therefore time derivatives of F an R in (2) can be neglected. Then, FDTD method has been used to solve (2), for F and R. As an example, the active layer thickness and width is given the values 150nm and 2μm, respectively. As shown in Fig .2, in order to optimize the DCC-DFB-SOA structure, the effects of r_κ and r_L on the transmitivitty and the transparency current are considered. Figure 2a demonstrates the effects of variations in r_κ, on the spectral range (δL) of this DCC-DFB-SOA by a constant r_L, while Fig. 2b illustrates the effects of variation in r_L on the spectral range (δL) by constant r_κ. For the conventional DFB-SOA case, the wavelength corresponding to the Bragg wavenumber experiences a great feedback and exhibits the greatest amplifier gain. However in the DCC-DFB-SOA, feedback for the input signal wavelength is changed when r_κ and r_L are introduced. This is because the Bragg wavelength is varied throughout the device. As a result of lower feedback, higher values of the transparent currents are required to realize the same peak transmission values. In order to understand the difference between the tramsmittivity of DCC-DFB-SOA with a conventional DFB-SOA, it is convenient to compare the curves of either r_L=1 and r_L=0 or r_κ=1 with the other curves presented in Fig. 2a and b. The best case of DCC-DFB-SOA which gives the valuable current (I=52.6mA) corresponds to r_κ=0.33 and r_L=0.5, where the conventional DFB-SOA gives the lower amount of 41.4mA.

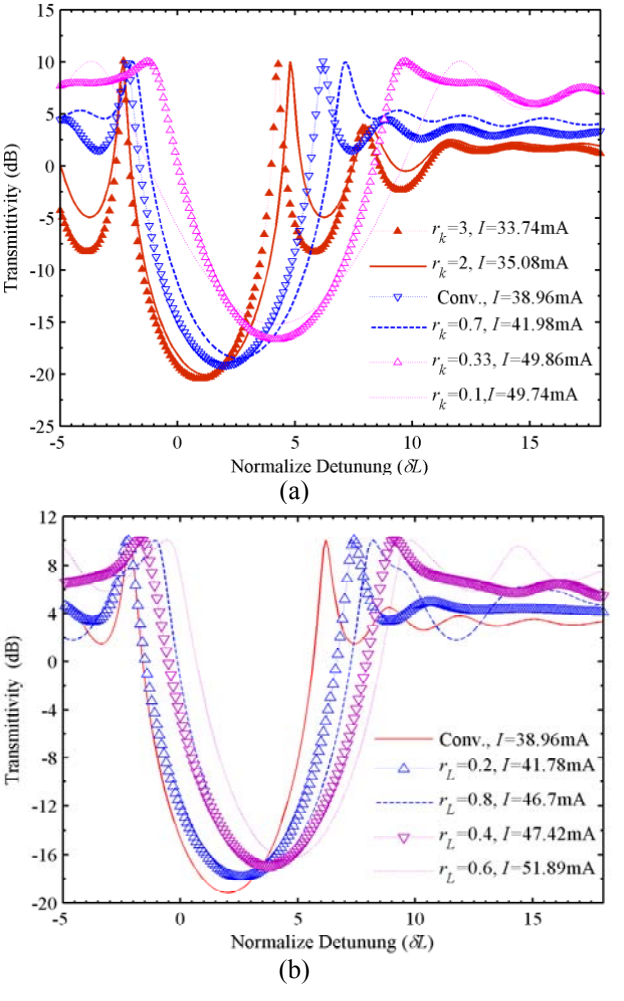

Fig. 2. Transmittivity versus Normalized detuning phase for (a) different coupling ratio with r_L=0. 5 and (b) different corrugation position with r_κ=0. 33.

The peak of transmitivitty at the Bragg resonance approaches infinity (in theory) where the current increases largely. This SOA reaches the transparency condition at which it operates output light without any input (i.e. SOA operates as a laser). As an example, the

threshold current of 75.15mA is obtained for transparency condition of the structure given in Fig. 3.

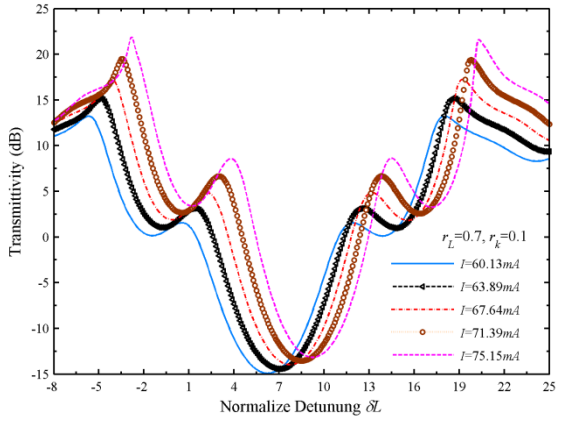

Fig. 3. Transmittivity versus Normalized detuning phase for different current values.

Now, In order to show the effects of r_L and r_κ on the transparency current, the device is simulated for different values of r_L and r_κ and results are shown in Fig. 4. The curves of Fig. 4 indicate that the designer can choose best values of r_L and r_κ for the maximum transparency current. However, very low values of r_κ, should be avoided which causes perturbation in the output intensity. Therefore, values r_κ=0.33 and r_L=0.5 are given, where the internal power is high, the speed is reasonable and no perturbation occurs.

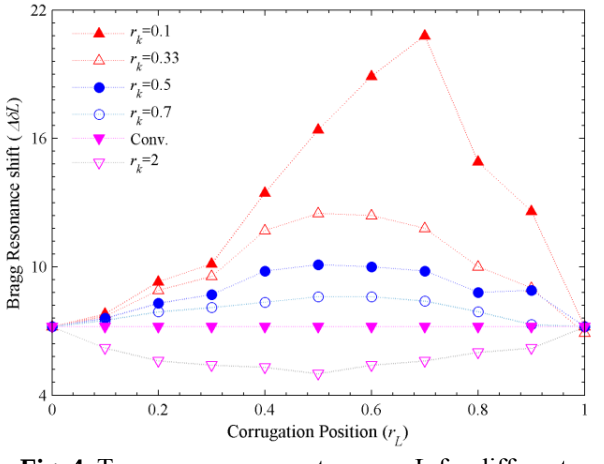

Fig. 4. Transparency current versus rL for different coupling ratio.

To trace out the bistable curve, first, the input power is increased and then the output power is calculated. Next the input power is decreased and the output power is recalculated. In spite of each round-trip time of 3ps (for L=300μm, $\Delta t=L/v_g$=3ps), a time period of (choose t=) 450ns is required for each input pulse to reach its steady state condition. Variation of the output power versus input power for different phase detuning, δL, are shown in Fig. 5. However, analysis of such behavior is not the main purpose of this work, but it is used in the flip-flop operation discussed in the following section.

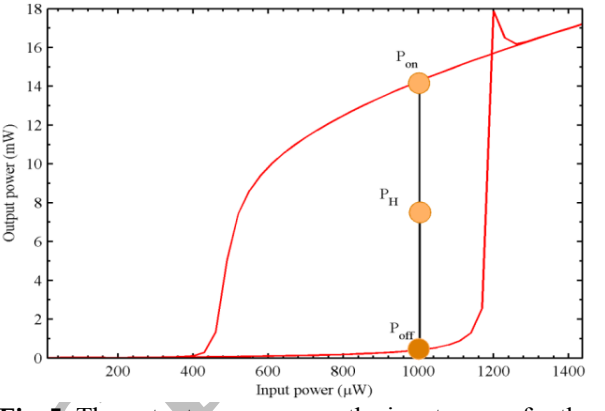

Fig. 5. The output power versus the input power for the different normalized detuning phase.

5. DYNAMIC RESPONSE BASED ON SPM

The two output states of an optical flip–flop based on optical bistability in a resonant type DCC-DFB-SOA are simply where the signal's input power intersects the two branches of the hysteresis curve, as shown in Fig. 5 at P_0=P_H. The output power of the signal can be set and reset between P_{on} and P_{off} by varying P_0 through the upward and downward switching thresholds, respectively.

The input power P_0 is initially located between the switching thresholds, like P_H in Fig. 5. Optical setting can be performed by increasing the input power beyond the upward switching threshold, and can be understood as follows: An increase in the optical power within the SOA stimulates recombination of electron-hole pairs (i. e. gain saturation), which increases the refractive index; the signal thereby increases its own wavenumber and optical phase. This self-phase modulation (SPM) shifts the photonic bandgap and Bragg resonances to longer wavelengths. As a Bragg resonance moves toward the signal wavelength, the internal optical power increases even more. Bistable upward switching occurs when a positive feedback loop (between the internal optical power, nonlinear refractive index and Bragg resonance) causes the Bragg resonance to shift through (? Shift towards, shift from…) the signal wavelength, providing resonant amplification for the signal. The set operation is shown in Fig. 6, where the time-dependent model based on the FDTD method has been used. This input power is given by [11]:

$$P_0 = P_H\left[1+0.5f(t-t_1)-0.5f(t-t_2)\right] \qquad (10)$$

Where the perturbation $f(t\text{-}t_x)$ to the average input power P_H is given by

$$f(t-t_x)=\exp\left\{-\left[(t-t_x)/Wf\right]^{2M}\right\} \qquad (11)$$

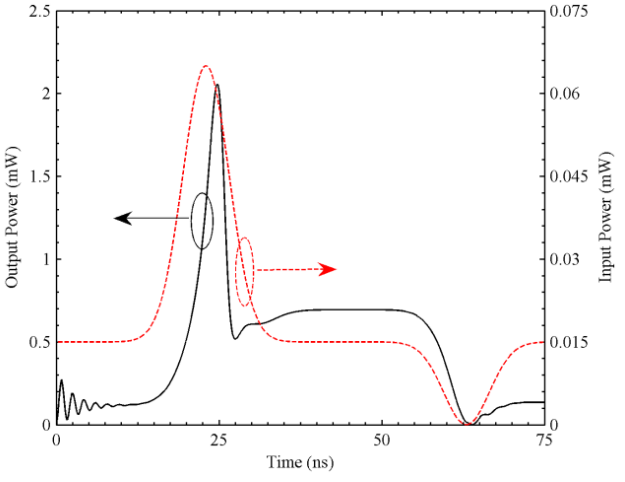

(a)

Fig. 6. (a) The output power and input power versus time with $\delta L=-1.5$ where the input power is multiplied by 10 for clarity. The energy of the set pulse is 0.3554fJ with FWHM=5ns and the energy of the reset pulse is 0.1066fJ with FWHM=5ns.

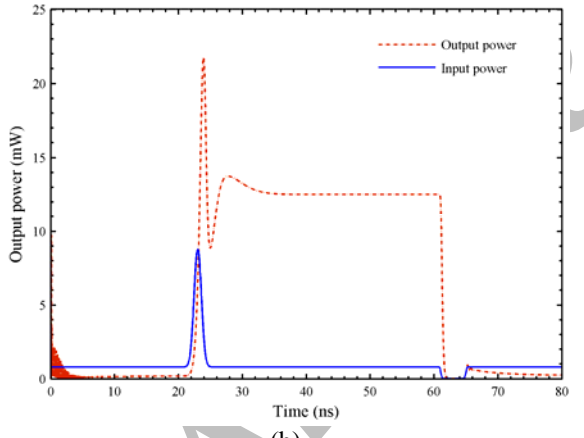

(b)

Fig. 6. (b) The output power and input power versus time with δL=10. The energy of the set pulse is 11.3437fJ with FWHM=0.8ns and the energy of the reset pulse is 3.0963fJ with FWHM=2ns.

Where the Wf is the pulse width and the M denote the Gaussian order, The signal's output power remains at a high level P_0 (corresponding to the upper hysteresis branch) even after its input power returns to the initial state P_H.

Dynamic response of the device for a constant carrier lifetime of (0.2ns) and for the case of effective carrier lifetime (as given in equation (8)) are calculated and plotted in Fig. 6 (a) and (b) respectively. As indicated in Fig. 6a in conventional DFB-SOA, in order to switch the device either from On to OFF or OFF to On state, a large value of full width half of maximum (FWHM) of either set or reset signal is needed. However, as indicated in Fig. 6b in a DCC-DFB-SOA, the value of FWHM is much lower than the case of conventional DFB-SOA. This is due to the greater current of the latter which is lower than the effective carrier lifetime.

Rise time, t_r, and fall time, t_f, in a flip-flop are calculated from %10 to %90 of hysteresis height and vice versa. In order to find the minimum values of t_r and t_f, first, the energy of set and reset pulses are increased and then the values for t_r and t_f are determined. The results are shown in Fig. 7. Increasing the peak of either the set or reset pulse, the internal power increases into the device which consequently raises the internal power. This action reduces the effective carrier lifetime and decreases t_r and t_f as shown in Fig. 7. As a result, the minimum value of t_r and t_f are obtained in the order of 45.3ps and 446.5ps, respectively. These values are smaller than the t_r and t_f of conventional DFB-SOA that are 1.45ns and 1.2ns respectively.

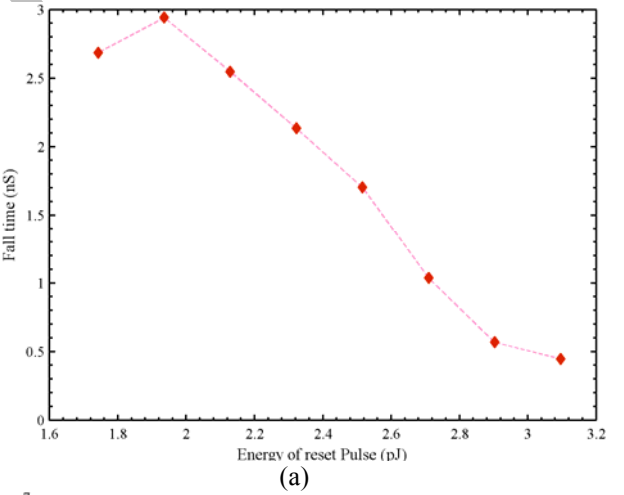

(a)

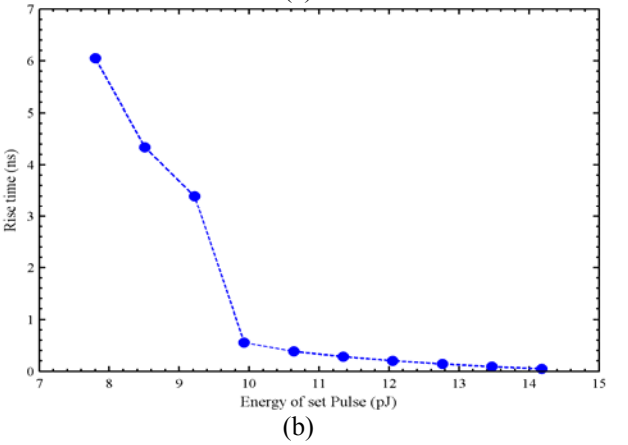

(b)

Fig. 7. (a) The rise and (b) fall times versus the energy of set and reset pulses.

6. CONCLUSIONS

In this paper, the dynamic response of the FF-DCC-DFB-SOA based on SPM mechanisms have been investigated. Also the effects of the energy of pulses on the rise and fall times are investigated. A modified FDTD method has been presented to study the effects of SPM on the dynamics response of FF-DFB-SOA. It has been found that in the DCC-DFB-SOA structure t_r and t_f are decreased in the order of 50ps and 500ps, respectively.

REFERENCES

[1] Takenaka M., Takeda K. and Nakano Y.; **"All-Optical Packet Switching and Label Buffering by MMI-BLD Optical Flip-Flop"**, *IEICE Electronics Exp*., Vol. 3, No. 15, pp 368 - 372, (2006)

[2] Maywar D. N., Agrawal G. P. and Nakano Y.; **"Robust Optical Control of an Optical-Amplifier-Based Flip–Flop",** *J. Opt. Soc. Am*. B, Vol. 6, No. 3, pp. 75 - 80, (2000)

[3] D'Oosterlinck W., Ohman F., Buron J., Sales S., P´erezPardo A., Ortigosa-Blanch A., Puerto G., Morthier G. and Baets R.; **"All-Optical Flip-Flop Operation Using a SOA and DFB laser Diode Optical Feedback Combination",** *J. Opt. Soc. Am. B*, Vol. 15, No. 10, pp. 6190 - 6199, (2007)

[4] Oosterlinck W. D', Buron J., Ohman F., Morthier G., and Baets R.; **"All-Optical Flip-Flop Based on an SOA/DFB-Laser Diode Optical Feedback Scheme",** *IEEE Photon. Technol. Lett*., Vol. 19, No. 7, pp. 489 - 491, (2007)

[5] Oosterlinck W. D', Morthier G., Baets R. and Erneux T.; **"Optical Bistability in a Traveling-Wave SOA Connected to a DFB Laser Diode: Theory and Experiment",** *IEEE J. Quantum Electron*, Vol. 42, No. 8, pp. 739 - 746, (2006)

[6] Kim Y., Kim J.H., Lee S., Woo D.H., Kim S.H. and Yoon T.H.; **"Broad-Band All-Optical Flip–Flop Based on Optical Bistability in an Integrated SOA/DFB-SOA",** *IEEE Photon. Technol. Lett*., Vol. 16, No. 2, pp. 398 - 400, 2004.

[7] Aleshams A., Moravvej-Farshi M.K., Heikhi M.H.; **"Tapered Grating Effects on Static Properties of a Bistable QWS-DFB Semiconductor Laser Amplifier",** *Solid-State Electronics*, Vol. 52, No. 1, pp. 156 - 163, (2008)

[8] L. Zhang, I. Kang, A. Bhardwaj, N. Sauer, S. Cabot, J. Jaques and D. T. Neilson; **"Reduced Recovery Time Semiconductor Optical Amplifier Using p-Type-Doped Multiple Quantum Wells",** IEEE Photon. Technol. Lett, Vol. 18, No. 22, pp. 2323 - 2325, (2006)

[9] H. Ghafouri-Shiraz; **Distributed Feedback Laser Diodes and Optical Wavelength Tunable Filters**, Distributed Feedback Laser Diodes and Optical Wavelength Tunable Filters, John Wiley and Sons, (2003)

[10] Park J., Li X., Huang W.P.**; "Performance Simulation and Design Optimization of Gain-Clamped Semiconductor Optical Amplifiers Based on Distributed Bragg Reflectors"**, *IEEE J. Quantum Electron*., Vol. 39, No. 11, pp. 1415 - 1423, (2003)

[11] Maywar D. N., Agrawal G. P. and Nakano Y.; **"All-Optical Hysteresis Control by Means of Cross-Phase Modulation in Semiconductor Optical Amplifiers",** J. Opt. Soc. Am. B, Vol. 18, No. 7, pp. 1003 - 1013, (2001)